RSC Advances

ROYAL SOCIETY OF CHEMISTRY

www.rsc.org/advances

Easy procedure to prepare Nitrogen-containing activated carbons for Supercapacitors

Article type: Full Paper

Information of correspond author:

Name: Xiaojuan Jin

Affiliation: MOE Key Laboratory of Wooden Material Science and Application, Beijing Key Laboratory of Lignocellulosic Chemistry, MOE Engineering Research Center of Forestry Biomass Materials and Bioenergy, Beijing Forestry University

Address:35 Qinghua East road, Haidian, 100083, Beijing, China

E-mail address: jxj0322@163.com

Tel.: +8613718160441

Fax: none

Author: Tongxin Shang

Mingyang Zhang

Xiaojuan Jin

Table of contents

Colour graphic

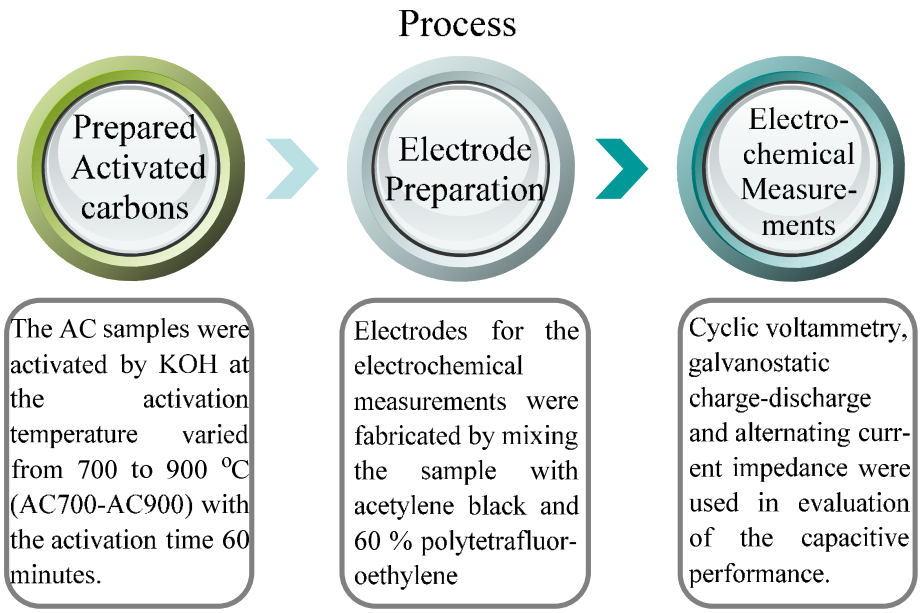

The urea-formaldehyde resin adhesive in waste medium density fiberboard play a role in modifying the activated carbons.

Easy Procedure to Prepare Nitrogen-containing Activated Carbons for Supercapacitors

Tong-Xin Shang[1], Ming-Yang Zhang[1], Xiao-Juan Jin[1,*]

1 MOE Key Laboratory of Wooden Material Science and Application, Beijing Key Laboratory of Lignocellulosic Chemistry, MOE Engineering Research Center of Forestry Biomass Materials and Bioenergy, Beijing Forestry University, 35 Qinghua East Road, Haidian, 100083, Beijing, China.

Abstract: Electrodes for the electrochemical measurements have been fabricated using activated carbons (AC) prepared by waste medium density fiberboard which was containing 12 % urea-formaldehyde resin adhesive of the mass. The AC samples were activated by KOH at the activation temperature varied from 700 to 900 ℃ (AC700-AC900) with the activation time 60 minutes. As the element analysis show, the nitrogen content of all the AC samples decreased from 2.42 % to 1.68 % with the increase of the activation temperature. The surface areas of the AC samples are range of 1308–1598 m^2/g, with higher microspore volume between 0.5 and 2.0 nm. In addition, as evidenced by galvanostatic charge-discharge curves, cyclic voltammetry and alternating current impedance measurements, AC electrodes show superior capacitive performances. The electrochemical double layer capacitor was measured in a 7 M KOH electrolyte, in which it was observed that the specific capacitances of AC700-AC900 varied from 176–232 F/g under the current density of 50 mA/g. The AC800 exhibited the best electrochemical behavior with a specific gravimetric capacitance of 232 F/g, with rectangular cyclic voltammetry curves at a scan rate of 2 mV/s, which remained at 211 F/g even at a current density of 10 A/g.

Key words: medium density fiberboard; supercapacitor; potassium hydroxide; electrochemical characteristics

* Corresponding author. Tel.: +8613718160441, Fax: None. E-mail address: jxj0322@163.com (Xiaojuan Jin).

1. Introduction

The idea of developing supercapacitors has attracted the attention of worldwide researchers due to their vast applications as power storage devices for electric vehicles, electronic appliances and memory back-up systems in computers. Supercapacitors have brought in as a new technical innovation which is unique and able to combine the energy properties of batteries with the power discharge characteristics of capacitors.[1] We can classify the supercapacitors into two types according to their energy storage mechanism, viz., redox supercapacitors and electrochemical double layer capacitors (EDLCs). EDLCs have emerged as a promising energy storage device for applications that need high power along with remarkable storage and cycle life. [2] As energy storage arises mainly from the accumulation of electronic and ionic charges at the interface between electrode materials and electrolyte solution in the EDLCs, the porosity and surface area of electrode active materials become the major factors that influence the specific capacitance of supercapacitors.[3] Porous carbon materials have been widely applied in many fields such as catalyst supports,[4] absorbents for bulky molecules,[5] biomedical devices,[6] and electrode materials.[7] Especially they can be directly used for electrode materials of electric double-layer capacitors[8] due to their high surface areas, large pore volumes, excellent conductivities, suitable pore sizes and textures, as well as chemical stability that can significantly improve the specific capacity, rate capability, and life cycle of energy storage systems.

However, the specific capacitance of activated carbon is much lower than theoretically expected, resulting in EDLCs with lower energy densities than predicted, which greatly hinders their practical application. As the research shown that [9] the higher capacitance is not only attribute to higher specific surface area, but also affected by the chemical surface composition of the carbon materials. The energy storage of EDLCs can be enhanced by enriching the surface of the carbon

materials with heteroatoms such as oxygen or nitrogen.[10~12] These heteroatoms modify the electron donor/acceptor properties of the carbon surface and are consequently expected to affect the charging of the electrical double-layer and yield pseudo-capacitance Faradaic reactions.[13] Various surface modification methods have been investigated to introduce heteroatoms onto the surfaces of carbon materials, for example, chemical, plasma, and flame treatments, coronal discharge, and direct fluorination.[14~18] Recently, nitrogen containing activated carbons (ACs) are subject of particular interest for researchers because they have shown a high versatility and efficiency in processing of waste products (in both gas and liquid phase, such as CO_2, NO_x, H_2S, SO_2, CH_4 and a wide range of organic compounds and heavy metals),[19~26] for obtaining excellent complexants and heterogeneous catalysts,[27, 28] as well as for the preparation of efficient capacitor materials.[29, 30] The methodologies most frequently used for the introduction of nitrogen functionalities to the structure of ACs, are: (a) by carbonization and further activation of polymer containing nitrogen in their structure,[31] and (b) by thermal treatment of carbon materials in the presence of nitrogen supplying agents such as ammonia, urea, melamine or nitrogen oxides.[32~34] In both cases the incorporated nitrogen can be found as pyridines, pyrrolidines, lactams, imides, amines or nitriles depending on the procedure. Moreover, a third procedure, consisting in the impregnation of the ACs with polyamines (e.g. polypropylenimine, [35] polyamidoamine [35] or polyethyleneimine (PEI) [36, 37]), which are nitrogenated molecules with a well-defined structure, has also been used. Although some of these methodologies are able to fix high nitrogen contents, all of them have important drawbacks. In particular, it is worth mentioning the requirements of high temperature and/or high pressure and the difficulty of understanding and controlling the reaction mechanisms.

We here describe the significance of a novel nitrogen rich carbon material, 'waste medium density fiberboard' (MDF) rejected by the furniture factory for supercapacitors. Medium density

fiberboard has rapidly increased in the past decade, replacing more and more solid wood lumber and plywood products. Since its first appearance in the 1960s, MDF has been steadily gaining market share worldwide. Meanwhile, in the international market, the MDF output of China is on the increase, reaching a record high of 50.23 million m^3 in 2012 according to the available data.[38] In 2001, the MDF output was 5.27 million m^3, which means the MDF output increase 8.53 times during the eleven years. MDF is a wood-based composite material used extensively in furniture production. With the rapid development in the production and usage of MDF, recycling of waste fiber has to be addressed. The sources of MDF byproducts include trimmings, dust generated by sanding of the panels and off-specification boards produced at a production facility, residues produced during remanufacturing and material removed from service at the end of its life-cycle. The traditional methods to manage byproducts from wood-based composites are by burning and landfilling. In China, waste MDF is usually burned to get heat energy, which is a kind of wasting of the resources, and more important, the poisonous gas containing nitrogen will be discharged in the atmosphere. Therefore, the development of methods for re-using the waste MDF materials is highly desired. The nitrogen atoms of the waste MDF originates from urea-formaldehyde resin adhesive used in the MDF manufacturing process, and some of nitrogen are further turned over to waste MDF-based ACs. The utilization of the waste MDF can significantly reduce the environmental impact and afford attractive products. To the best of our knowledge, there is little literature of synthesizing such an activated carbon material for supercapacitors.

In this paper, we report an efficient and straightforward methodology directed to prepared nitrogen containing activated carbons by waste MDF, which with high specific surface area and considered to be a novel nitrogen rich carbon material for high-performance electrode preparation. As we known, MDF is wood-based material made from lignocellulosic fibers bonded together by

synthetic resin (usually urea-formaldehyde) under heat and pressure. MDF usually contains 10–12 % urea-formaldehyde resin adhesive which is enriched by nitrogen, after carbonization and activation the nitrogen heat stabled are reserved. The study has been focused on the procedure to improve the capacitive performance of all carbon samples, remarking the effect of activation temperature on the electronic performance of MDF-based activated carbons. In addition, several measurements were introduced to describe the characterization of MDF-based activated carbons and carbon electrodes.

2. Material and Methods

2.1 *Materials*

The waste MDF was kindly provided by Beijing Jiahekailai Furniture and Design Company, which was obtained in the furniture manufacturing process containing 12 % urea-formaldehyde resin adhesive of the mass. Other chemicals were analytical grades and were purchased from Beijing Lanyi Chemical reagent. Double distilled water was used for preparation of all required solutions.

2.2 *Preparation of activated materials*

The carbonization process was carried out in a high-purity nitrogen atmosphere at the temperature increase rate of 10 ℃/min to the final temperature of 500 ℃, separately, maintained for 60 min. The sample were then ground and screened out with sieves. The fraction in the particle diameter ranged from 40 meshes to 60 meshes. The particle sample was dried in a 105 ℃ oven for 8 h; in activation step, 3 grams of the oven-dried samples were soaked in a 50 % KOH solution for 16 h at the mass ratio impregnation (3:1). The samples were then activated at the temperature 700, 750, 800, 850, 900 ℃ for 60 min in nitrogen atmosphere. The obtained activated carbons (AC700, AC750, AC800, AC850 and AC900) were boiled first with 1 M HCl solution and then with distilled water

until the pH of solution reach to about 6–7. Finally, these activated carbons were dried at 105 ℃ in an oven for 8 h.

2.3 *Characterization of the activated carbon*

2.3.1 *Chemical surface composition*

Chemical surface composition and state of the samples were determined by elemental analysis and X-ray photoelectron spectroscopy (XPS). (i) The elemental analysis (contents in carbon, hydrogen, and nitrogen) of the activated carbons was under taken in a CHNS Analyzer (Thermofinnigan Flash, EA, 1112 series). (ii) XPS was performed on an ESCALAB250 (VG Scientific, UK) using a monochromatic Al K_α radiation. The acceleration tension and power of X-ray source were 15 kV and 100 W, respectively. The sample charging was corrected by using the C1s peak (284.6 eV) as an internal standard. The surface atomic ratios were calculated from the ratio of the corresponding peak areas after correction with the theoretical sensitivity factors based on the Scofield's photoionization cross-sections.

2.3.2 *Porous Texture*

The N_2 adsorption-desorption isotherms of activated carbon prepared under optimum conditions were measured with an accelerated surface area and porosimetry system (ASAP 2010, Micromeritics) for determining the surface areas. Prior to the measurements, the samples were outgassed at 573 K, under nitrogen flow for at least 2 h. The nitrogen adsorption-desorption data were recorded at a liquid nitrogen temperature of 77 K. The nitrogen adsorption isotherm was measured over a relative pressure (p/p_0) range, from approximately 10^{-6} to 1. The Brunauer-Emmett-Teller (BET) surface area was calculated using the BET equation from the selected N_2 adsorption data, within a range of relative pressure, p/p_0, from 0.1 to 0.3. Pore size distribution in the micropore range was obtained by the Barrett-Joyner-Halenda (BJH) method.

2.4 *Electrode preparation and electrochemical measurements*

2.4.1 *Electrode preparation*

The dried activated carbon samples including AC700, AC750, AC800, AC850 and AC900 were grinded in an agate mortar. Electrodes for the electrochemical measurements were fabricated by mixing the sample with acetylene black and 60 % polytetrafluoroethylene in a mass ratio of 87:10:3 and dispersed in C_2H_5OH aqueous solution forming homogeneous slurry. The slurry was then pressed into the nickel foam (square, about 1 cm^2) under a pressure of 20 MPa with a nickel tape for connection to one disk.

2.4.2 *Electrochemical measurements*

The capacitive performance of all carbon samples was investigated in 7 M KOH using two-electrode cells. The electrodes were dried at 105 ℃ in an oven for 8 h and then weighted. The two electrodes with identical weight were selected for the measurements. Cyclic voltammetry, galvanostatic charge-discharge and alternating current impedance were used in evaluation of the capacitive performance. Constant current density charge-discharge and rate performance were tested using the BT2000 battery testing system (Arbin Instruments, USA) at room temperature. Besides, as for the charge-discharge the specific capacitance of the electrode can also be calculated according to the following equation:

$$C_m = \frac{I \times \Delta t}{\Delta V \times m} \quad (1)$$

Where C_m is the specific capacitance per mass weight activated carbon in the electrode (F/g), I is the discharge current (A), Δt is the time elapsed for the discharge branch from 0 to 1 V (s), ΔV is the voltage difference within the time (V) and m is the active mass of carbon on the electrode (g).

Cyclic voltammetry (CV) and alternating current impedance were employed for the electrochemical measurements of each sample using the 1260 electrochemical workstation (Solartron

Metrology, UK) at room temperature. The gravimetric capacitance (C_m) analyzed, which mean the specific capacitance per mass weight activated carbon in the electrode, is expressed in F/g and calculated by the following formulas of (2) and (3):

$$C = \frac{Q}{U} = \frac{Q}{t} \times \frac{t}{U} = I \times \frac{t}{U} = \frac{I}{U/t} \quad (2)$$

$$C_m = \frac{C}{m} = \frac{I/m}{U/t} = \frac{I/m}{v} \quad (3)$$

Where I is observed value (A), m is average weight of each activated carbon disk (g) and v is the voltage scan rate (mV/s).

3. Results and discussion

3.1 *Elemental analysis*

Since the surface features are considered as very important for the performance of carbonaceous materials as supercapacitors, the changes in the texture and chemistry of the composites are first analyzed to be further linked to the electrochemical performance.

Table 1 – The elemental analysis of the raw material, carbonization and AC samples.

Sample	CHN (wt %)		
	N (%)	C (%)	H (%)
C0	8.39	45.16	5.76
C500	6.81	74.50	2.69
AC700	2.42	63.27	1.67
AC750	2.35	74.87	1.47
AC800	2.09	85.96	1.73
AC850	1.89	88.84	1.36
AC900	1.68	90.25	0.84

The extensive studies on the chemistry of nitrogen modified carbons revealed the dependence of the surface functionality on the pyrolysis temperature.[39~42] The carbon pyrolyzed is expected to have nitrogen mostly in the form of amine, amide, and ammonium.[43] During pyrolysis, these groups decompose; some nitrogen is released while some is incorporated into the carbon matrix. Table 1 shows the elemental analysis of the raw material C0, carbonized sample C500 and AC samples, respectively. It shows that the initial material C0 contains some nitrogen functionalities coming from the decomposition of the urea-formaldehyde resin adhesive used for its preparation. After activation, it is can be seen that as temperature increased, there is a sharp increase in the element of C and a decrease in H and N contents. Nitrogen is present in all AC samples ranging typically from 1.68 % to 2.42 %, which suggest some of the nitrogen atoms of the waste MDF originate from urea-formaldehyde resin adhesive used in the MDF manufacturing process further turned over to waste MDF-based ACs.

3.2 *XPS study*

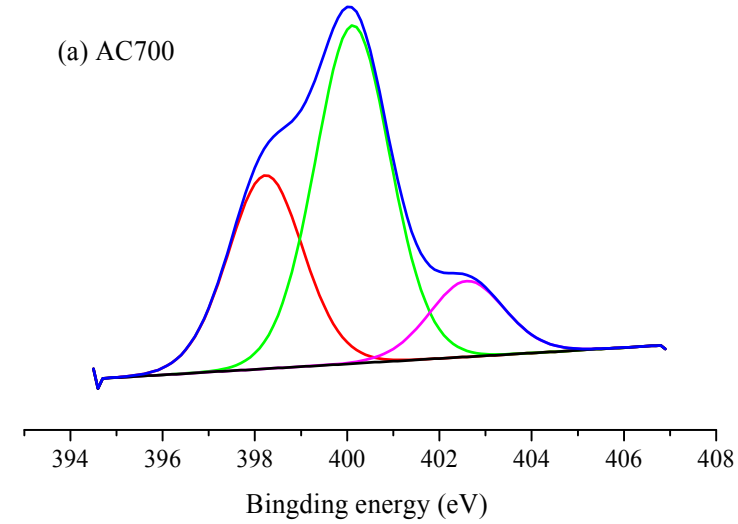

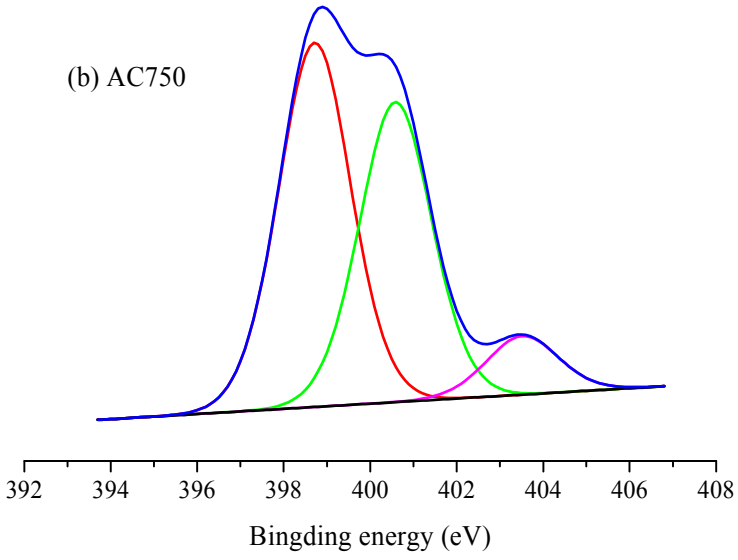

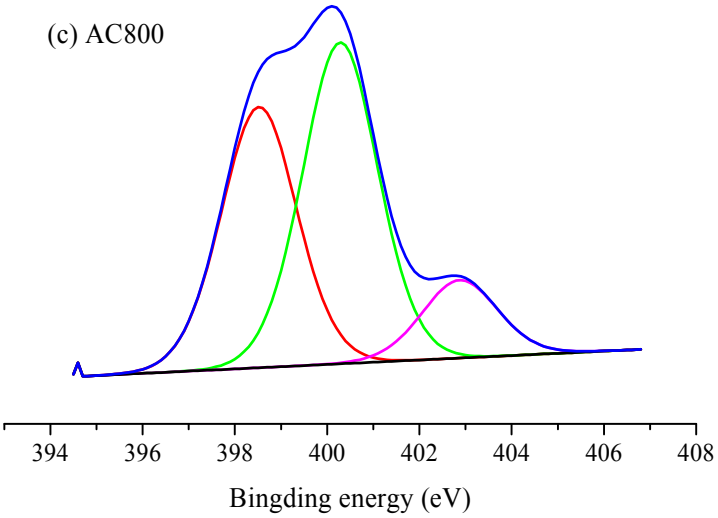

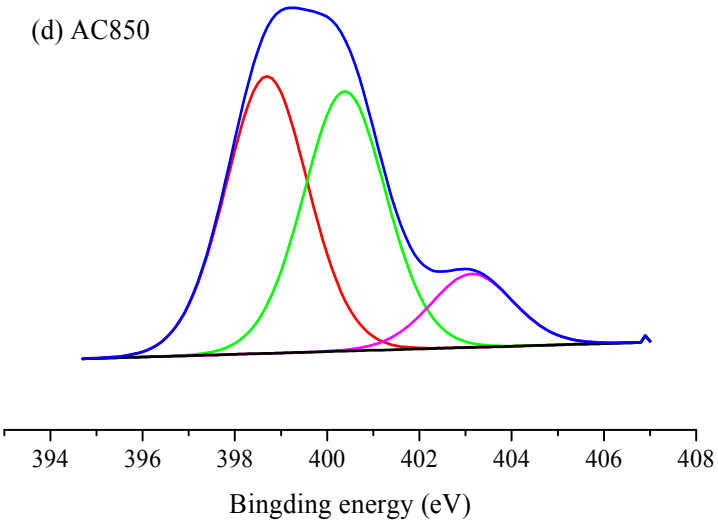

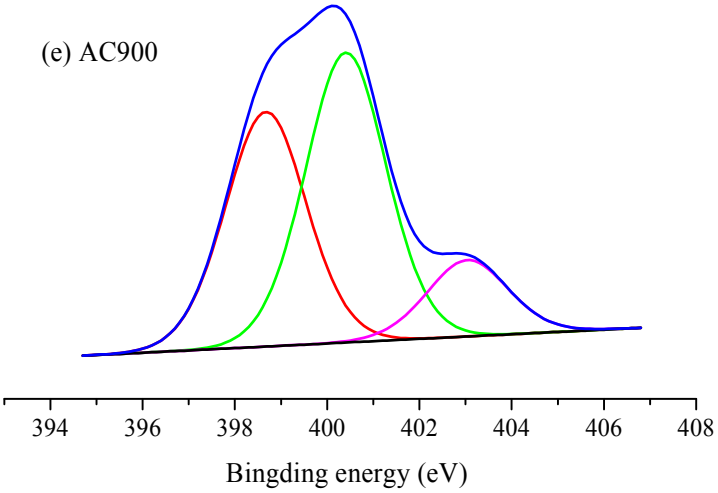

Fig. 1 – Fitted high-resolution XPS N1s spectra of the AC samples.

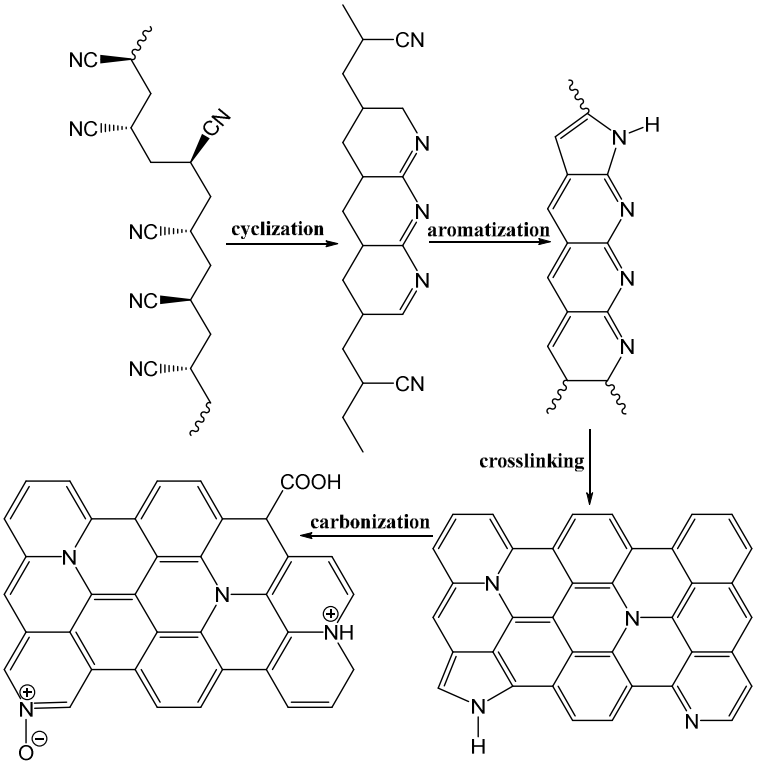

Fig. 2 – Scheme of the graphitization of carbon materials.

Table 2 – Distribution of N species obtained from the deconvolution of the N1s peaks.

Sample	N-6, Pyridinic nitrogen (%) (398.7 ± 0.3eV)	N-5/N-P, Pyrrolic nitrogen, pyridone (%) (400.3 ± 0.3 eV)	N-Q, Quaternary nitrogen (%) (401.4 ± 0.4 eV)	N-X, Oxidized nitrogen (%) (402 ~ 405 eV)
AC700	36.86	55.67	-	8.47
AC750	45.41	46.50	-	8.09
AC800	46.52	41.69	-	11.79
AC850	48.40	39.56	-	12.03
AC900	49.06	38.24	-	12.70

To further understand the surface chemistry of the AC samples, the nature of N species at the surface of the AC samples was investigated by the XPS measurement. The N1s XPS spectra of AC samples are demonstrated in Fig. 1. According to the literatures,[31~32, 44~49] the chemical state of nitrogen atoms in graphene layers could be assigned four types: N-6 (pyridinic nitrogen, which bonds with two C atoms with one p-electron localized in the π conjugated system; 398.7 ± 0.3 eV), N-5/N-P (pyrrolic nitrogen which bonds with two C atoms with two p-electrons/pyridinic nitrogen in association with oxygen functionality marked pyridine; 400.3 ± 0.3 eV), N-Q (quaternary nitrogen, nitrogen substituted with carbons in the aromatic grapheme structure, 401.4 ± 0.4 eV), N-X and oxidized nitrogen (402 ~ 405 eV). As Fig. 1 shows, except for the N-Q, all nitrogen functionalities are located at the edge of the graphene structure. The relative contributions of each nitrogen species to the total peak area are summarized in Table 2. The results indicate that the chemical state of nitrogen could be sensitively varied by the carbonization temperature, with the increasing of the temperature, there is an increase in pyridinic nitrogen and oxidized nitrogen and a decrease in pyrrolic nitrogen and

pyridone. J R Pels et al.[41] also drew the same conclusion and our conclusion corresponds with the analysis of Claudia Weidenthaler et al.[50] According to the analysis, under mild pyrolysis conditions the cyclization and aromatization, as schematically shown in Fig. 2, is not completed but already occurred partially. Meanwhile, N-X species are also present but only in low amounts. As the temperature increased, the aromatic extended present and the total amount of nitrogen is slightly reduced, but a large fraction of N-5 nitrogen is transformed into N-X. Under severe pyrolysis conditions, N-6 and N-X increased as N-5 decreased. For a small part it is released in the volatiles, but the majority is converted to N-6 and N-X, with the latter as the major constituent.

3.3 *Textural studies of ACs*

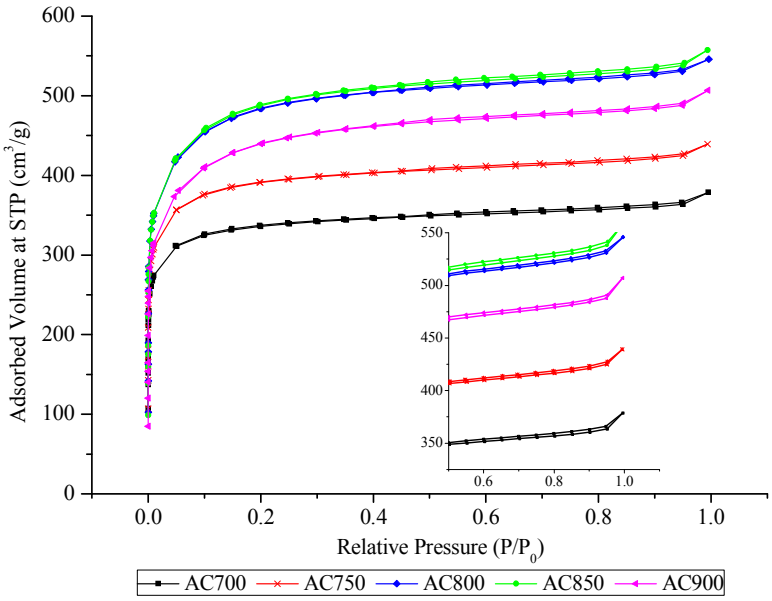

Fig. 3 – Nitrogen adsorption-desorption isotherms for prepared activated carbons by KOH activation.

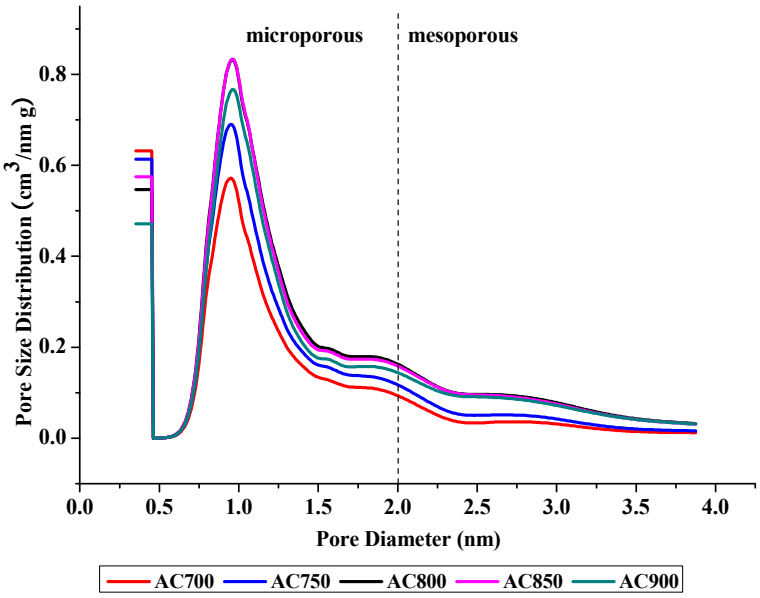

Fig. 4 – Pore size distributions of prepared activated carbons.

Table 3 – Physical properties of the ACs.

Sample	S_{BET} (m^2/g)	S_{mi} (m^2/g)	V_{tot} (cm^3/g)	V_{mi} (cm^3/g)	S_{me} (%)	V_{me} (%)
AC700	1308	1255	0.586	0.505	4.10	13.81
AC750	1505	1443	0.679	0.588	4.14	13.43
AC800	1586	1499	0.795	0.688	5.47	13.40
AC850	1598	1508	0.862	0.737	5.66	14.49
AC900	1424	1334	0.784	0.663	6.35	15.47

The N_2 adsorption-desorption isotherms, as shown in Fig. 3, which is used to determine the surface area and pore-size distribution of the ACs. The isotherms of all AC samples resembles a combination of type-I and type-II isotherms, in accordance with the International Union of Pure and Applied Chemistry (IUPAC) classification. This adsorption behaviour exhibits a combination of microporous-mesoporous structure. Meanwhile, the isotherm shows an apparent hysteresis loop (H4

type) in the desorption branch at relative pressures above 0.8, indicating the presence of mesopores.[51] The hysteresis loop is usually associated with the filling and emptying of the mesopores by capillary condensation.[52] With increasing the activation temperature from 700 to 850 ℃, the adsorption increased and with increasing the activation temperature from 850 to 900 ℃, the adsorption decreased. To my knowledge, higher activation temperature often follows faster reaction, leads to a larger BET specific surface area, and thus contributes larger nitrogen adsorption capacity. However, when the activation temperature reached 850 ℃, the nitrogen adsorption capacity decreased. It was probably that when the activation temperature reached a certain value, the pores would be widened and burnt off so that the BET specific surface area decreased. As shown in Fig. 4, the curve of AC850 is located in the top, which indicate that it has the highest microspore and mesopore volume. The parameters of the porous texture of ACs calculated from the isotherms are presented in Table 3. As observed in Table 3, the AC850 has the biggest BET surface area 1598 cm^3/g and the biggest total volume 0.862 cm^3/g, which correspond to the results of Fig. 4 that shows the pore size distribution of the ACs. As we know, micropores are less than 2 nm wide, mesopores are 2–50 nm wide, and macropores are more than 50 nm wide. As can be seen from Fig. 4, the sharpest peaks occurred at pore diameter above 1.0 nm, shows that a majority of the pores fall into the range of micropores. Meanwhile, Fig. 4 shows that the pore size of all the prepared samples included a small amount of mesopores, which corresponds to the analysis results of the N_2 adsorption-desorption isotherms in Fig. 3.

3.4 *Electrochemical characteristics*

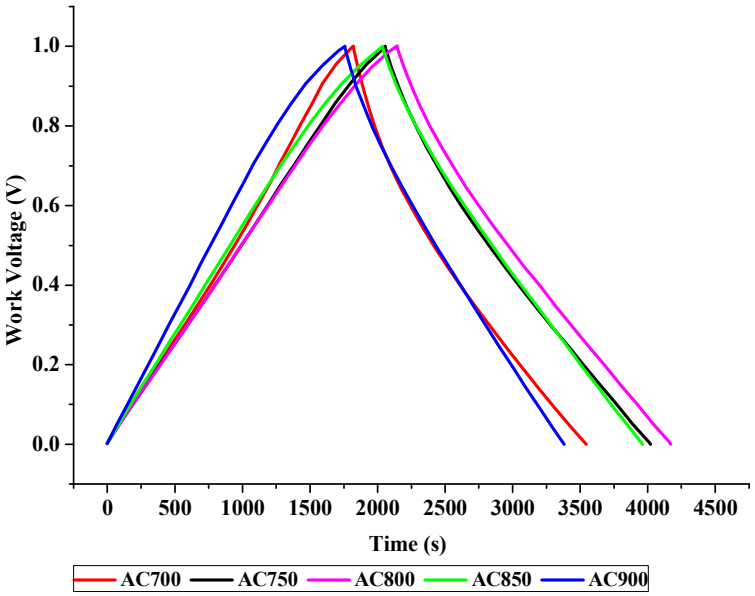

Fig. 5 – Charge-discharge curves of AC electrodes in 7 M KOH at a constant current density of 50 mA/g.

The galvanostatic charge-discharge curves of the AC electrodes at a current density of 50 mA/g are presented in Fig. 5. All the charge-discharge curves exhibit triangular shapes, with low IR drops, indicating typical capacitive behavior.[53] Besides, it is also observed that the AC samples display straight discharge slopes which indicate excellent discharge capabilities and highly stability and reversibility feature. The AC samples with different activation temperature, AC800 exhibited the best capacitive behavior, it is due to the big BET surface area and the high microspore and mesopore volume, which is beneficial to the access of the electrolyte into the pore volume and consequently improve ionic transport in EDLCs.[54] Additionally, the corresponding specific capacitance values at a current density of 50 mA/g are calculated by the equation (1). The specific capacitance of the AC700-AC900 varied from 176–232 F/g (AC700: 199 F/g, AC750: 214 F/g, AC800: 232 F/g, AC850: 221 F/g, AC900: 176 F/g) under this current density. Compared AC850 with AC800, AC850 has the higher specific surface area and amount of mesopores, but lower capacitance, which is probably due to that AC800 has the higher nitrogen (2.09 %) than AC850 (1.89 %). Moreover, the

specific surface area of AC850 is much bigger than that of AC750, however the two samples exhibited the similar capacitive behavior. The results also indicate that the higher capacitance is not only attribute to higher specific surface area and amount of mesopores, but also the existence of nitrogen. The presence of mesopores can enhance utilization of the exposed surface for charge separation and provide resistance pathways for the ions through the porous particles,[9] but it can not enhance the capacitance infinitely. At this point, the existence of nitrogen shows great advantage.

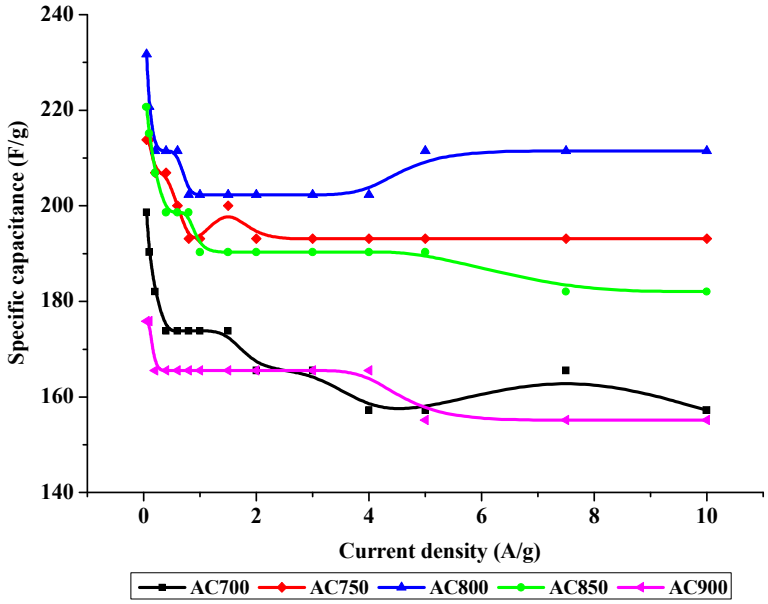

Fig. 6 – Calculated specific capacitance as a function of current density of AC electrodes.

The galvanostatic charge-discharge measurements were further carried out at various current densities ranged from 0 to 10 A/g within the potential window from 0 to 1 V to calculate the specific capacitances of all AC samples, and the results are collected in Fig. 6. Obviously, a sudden potential drop at the very beginning of the constant current discharge is usually observed for EDLCs and this drop has been designated as the IR drop, which can be attributed to the resistance of electrolyte solution and the inner resistance of ion diffusion in carbon micropores.[9, 55] From Fig. 6, it can be seen that the capacitance decreased with current density to a similar extent for all of the

samples. However, the IR drop of the sample AC750 is slightly smaller than AC850 due to its high nitrogen. An opposite effect is found for the carbon, for which about 10 % decrease in the capacitance is found. This can be linked to a decreased pseudo-capacitive contribution as a result of the removal of nitrogen containing groups. In addition, for the sample AC800 and AC850, the sample with the higher capacitance was not the sample with the higher BET surface area. Therefore, other factors, apart from the surface area, must be contributing to the enhancement of capacitance.[56] It is revealed that the nitrogen groups in the AC samples can improve the performance of the capacitance.

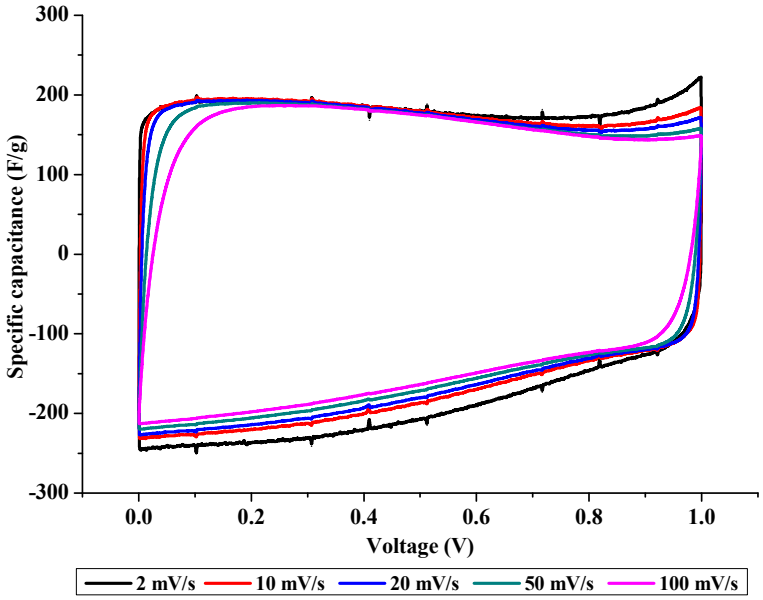

Fig. 7 – Cyclic voltammograms of AC800 electrode in 7 M KOH at different scan rate

Owing to AC800 with more attractive feature of highly interconnected porosity and higher surface area, higher specific capacitance, cyclic voltammogram tests from 2 to 100 mV/s between 0 and 1 V were investigated to gain a qualitative understanding of the influence of pore structure on the rate dependence of the charge-discharge behavior. At 2, 10, 20, 50 and 100 mV/s, the curves present the quasi rectangular shapes for the charge/discharge processes. At the highest scan rate 100 mV/s, a rectangular shape with only slight deviation from the ideal rectangular shape can be observed. Cyclic

voltammetry in a two-electrode configuration is an excellent technique for studying the presence of pseudo-capacitive phenomena. Materials with pseudo-capacitance show redox peaks related to electron-transfer reactions. The voltammograms in Fig. 7 show the redox processes which are the contribution of the nitrogen groups in AC samples. In addition, a small hump during the sweep at 0.8–1.0 V was clearly observed for the AC800 sample, which is usually attributed to pseudo-faradaic reactions involving the quinone functional groups. The nitrogen functional groups, especially the pyrrolic and pyridinic nitrogen have been reported to be electrochemically active in the pseudo-faradaic reactions. It is believed that this kind of behavior is additionally enforced by electron-donating effect of nitrogen heteroatoms. It also suggests that AC800 can be an excellent candidate as electrode materials for supercapacitor.

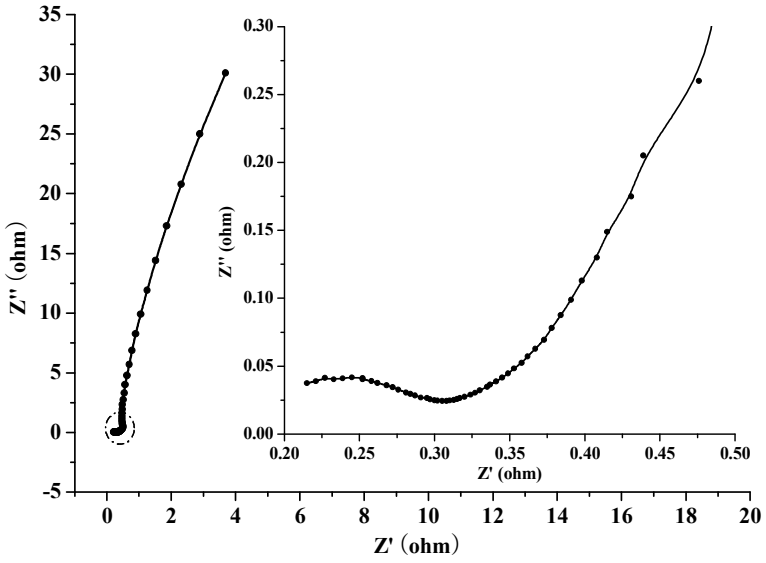

Fig. 8 – Nyquist polt of AC800 electrodes (inset: enlarged high-frequency region of Nyquist polt)

Electrochemical impedance spectroscopy (EIS) was utilized to obtain information on the supercapacitors performance, such as Fig. 8. Their frequency dependence and equivalent series resistance (ESR)[57] in Fig. 8 illustrates the Nyquist plots of the AC800 super capacitors**.** A semicircle

of very small radius was obtained at high-frequency region and a straight line in the low frequency region. At very high frequencies, the intercept at the real axis is the ESR value; the ESR value of AC800 was about 0.21. The imaginary part of the impedance spectra at low frequencies represents the capacitive behavior of the electrode and approaches a 90◦ vertical line in an ideal capacitor. Obviously, the straight line part of carbon AC800 is more close to vertical line along the imaginary axis, suggesting AC800 has good capacitive behavior. The sample of AC800 showed a semicircle in the mid-high frequency zone, which is related to the high intrinsic electrical resistance and faradaic reactions. This resistance results in a high kinetic dependence upon faradaic phenomena with current density. This may be attributed to pseudo-faradaic reactions involving the quinone functional groups and the nitrogen functionalities.

4. Conclusion

N-enriched electrode materials for supercapacitors were prepared from medium density fiberboard base by KOH activation. The effects of physical properties and chemical composition of waste MDF-based ACs on the electrochemical performance were explored. The porosity characterization results showed that all of the ACs produced are essentially microporous. Activated carbon with a highest surface area and mesopore volume was produced when the activation temperature was 850 ℃, then the better activation temperature was 800 ℃. Include the influence of nitrogen content, the activated carbon AC800 exhibited the best electrochemical behavior with rectangular cyclic voltammetry curves at a scan rate of 2 mV/s, with a specific gravimetric capacitance of 232 F/g at constant current densities of 50 mA/g, which remained at 211 F/g even at a current density of 10 A/g. Correlating the capacitive behavior with textural characteristics, the good electrochemical properties were ascribed to the high surface area, wide pore size distribution and

nitrogen functionalities. Therefore, the N-containing AC based on medium density fiberboard is a simple and efficient way to enhance the performance of AC-based EDLCs.

Acknowledgment:

This study was funded by State Forestry Administration under Project 201204807: the study on the technology and mechanism of the activated carbon electrode preparation from waste hard board.

Reference

[1] S.K. Chang, Z. Zainal, K.B. Tan, N.A. Yusof, W.M.D.W. Yusoff, S.R.S. Prabaharan, Curr. Appl. Phys. 2012, 12, 1421–1428.

[2] J.R. Miller, A.F. Burke, J. Electrochem. Soc-Interf. 2008, 17, 53–57.

[3] H. Wu, X.Y. Wang, X.Y. Wang, X.Y. Zhang, L.L. Jiang, B.N. Hu, Y.P. Wang, J. Solid. State. Electrochem. 2012, 16, 2941–2947.

[4] J.S. Yu, S. Kang, S.B. Yoon, G. Chai, J. Am. Chem. Soc. 2002, 124, 9382–9383.

[5] X. Zhuang, Y. Wan, C.M. Feng, Y. Shen, D.Y. Zhao, Chem. Mater. 2009, 21, 706–716.

[6] A. Vinu, M. Miyahara, V. Sivamurugan, T. Mori, K. Ariga, J. Mater. Chem. 2005, 15, 5122–5127.

[7] C. Vix-Guterl, E. Frackowiak, K. Jurewicz, M. Friebe, J. Parmentier, F. Béguin, Carbon 2005, 43, 1293–1302.

[8] K.S. Xia, Q.M. Gao, J.H. Jiang, J. Hu, Carbon 2008, 46, 1718–1726.

[9] X.H. Wu, X.T. Hong, J.M. Nan, Z.P. Luo, Q.Y. Zhang, L.S. Li, H.Y. Chen, K.S. Hui, Micropor. Mesopor. Mat. 2012, 160, 25–31.

[10] G. Milczarek, A. Ciszewski, I. Stepniak, J. Power Sources 2011, 196, 7882–7885.

[11] H. Tamon, M. Okazaki, Carbon 1996, 34, 741–746.

[12] A.T. Christopher, W.E. Marshall, M.M. Johns, Carbon 1999, 37, 1207–1214.

[13] T. Savage, S. Bhattacharya, B. Sadanadan, J. Gaillard, T.M. Tritt, Y.P. Sun, Y. Wu, S. Nayak, R. Car, N. Marzari, P.M. Ajayan, A.M. Rao, J. Phys-Condens. Mat. 2003, 15, 5915–5921.

[14] A. Felten, C. Bittencourt, J.J. Pireaux, Nanotechnology 2006, 17, 1954–1959.

[15] T. Hoshida, D. Tsubone, K. Takada, H. Kodama, T. Hasebe, A. Kamijo, T. Suzuki, A. Hotta, Surf. Coat. Tech. 2007, 202, 1089–1093.

[16] Z. Hruska, X. Lepot, J. Fluorine. Chem. 2000, 105, 87–93.

[17] Y. Hattori, H. Kanoh, F. Okino, H. Touhara, D. Kasuya, M. Yudasaka, S. Iijima, K. Kaneko, J. Phys. Chem. B 2004, 108, 9614–9618.

[18] E. Frackowiak, Phys. Chem. Chem. Phys. 2007, 9, 1774–1785.

[19] J.S. Mattson, H.B. Mark, Activated carbon: Surface chemistry and adsorption from solution, Marcel Dekker Publisher, New York, 1971, p. 209–221.

[20] W.J. Lyman, Applicability of carbon adsorption to the treatment of hazardous industrial wastes, Carbon adsorption handbook, Ann Arbor Science Publishers, Inc. 4, 1978, pp. 131–165.

[21] C.L. Mangun, J.A. DeBarr, J. Economy, Carbon 2001, 39, 1689–1696.

[22] Y.F. Jia, B. Xiao, K.M. Thomas, Langmuir 2002, 18, 470–478.

[23] M. Sevilla, P. Valle-Vigón, A.B. Fuertes, Adv. Funct. Mater. 2011, 21, 2781–2787.

[24] M.S. Shafeeyan, W.M.A.W. Daud, A. Houshmand, A. Arami-Niya, Appl. Surf. Sci. 2011, 257, 3936–3942.

[25] S. Fatemi, M. Vesali-Naseh, M. Cyrus, J. Hashemi, Chem. Eng. Res. Des. 2011, 89, 1669–1675.

[26] P. Nowicki, R. Pietrzak, Chem. Eng. J. 2011, 166, 1039–1043.

[27] C. Hajji, R. Haag, Hyperbranched polymers as platforms for catalysts, Springer Berlin Heidelberg, Berlin, 2006, p. 149–176.

[28] P.H. Li, L. Wang, Adv. Synth. Catal. 2006, 348, 681–685.

[29] D. Hulicova-Jurcakova, M. Seredych, G.Q. Lu, T.J. Bandosz, Adv. Funct. Mater. 2009, 19, 438–447.

[30] K. Jurewicz, K. Babel, Energy Fuel 2010, 24, 3429–3435.

[31] J. Lahaye, G. Nanse, A. Bagreev, V. Strelko, Carbon 1999, 37, 585–590.

[32] A. Bagreev, J.A. Menendez, I. Dukhno, Y. Tarasenko, T.J. Bandosz, Carbon 2004, 42, 469–476.

[33] J.P. Boudou, M. Chehimi, E. Broniek, T. Siemieniewska, J. Bimer, Carbon 2003, 41, 1999–2007.

[34] P. Garćia, J.F. Espinal, C. Salinas Martínez de Lecea, F. Mondragón, Carbon 2004, 42, 1507–1515.

[35] T. Gao, E.S. Tillman, N.S. Lewis, Chem. Mater. 2005, 17, 2904–2911.

[36] C.Y. Yin, M.K. Aroua, W.M.A.W. Daud, Colloid Surface A 2007, 307, 128–136.

[37] M. Owlad, M.K. Aroua, W.M.A.W. Daud, Bioresource Technol. 2010, 101, 5098–5103.

[38] S.H. Chen, International Wood Industry 2013, 7, 23–25.

[39] S. Bashkova, T.J. Bandosz, J. Colloid. Interf. Sci. 2009, 333, 97–103.

[40] R.J.J. Jansen, H. Van Bekkum, Carbon 1995, 33, 1021–1027.

[41] J.R. Pels, F. Kapteijn, J.A. Moulijn, Q. Zhu, K.M. Thomas, Carbon 1995, 33, 1641–1653.

[42] K. Stańczyk, R. Dziembaj, Z. Piwowarska, S. Witkowski, Carbon 1995, 33, 1383–1392.

[43] F. Adib, A. Bagreev, T.J. Bandosz, Langmuir 2000, 16, 1980–1986.

[44] K. Jurewicz, K. Babel, A. Ziólkowski, H. Wachowska, Electrochim. Acta. 2003, 48, 1491–1498.

[45] K. Jurewicz, K. Babel, A. Ziólkowski, H. Wachowska, J. Phys. Chem. Solids. 2004, 65, 269–273.

[46] F. Kapteijn, J.A. Moulijn, S. Matzner, H.P. Boehm, Carbon 1999, 37, 1143–1150.

[47] Y.J. Kim, Y. Abe, T. Yanagiura, K.C. Park, M. Shimizu, T. Iwazaki, S. Nakagawa, M. Endo, M.S. Dresselhaus, Carbon 2007, 45, 2116–2125.

[48] J. Machnikowski, B. Grzyb, J.V. Weber, E. Frackowiak, J.N. Rouzaud, F. Béguin, Electrochim. Acta. 2004, 49, 423–432.

[49] M. Vujković, N. Gavrilov, I. Pašti, J. Krstić, J. Travas-Sejdic, G. Ćirić-Marjanović, S. Mentus, Carbon 2013, 64, 472–486.

[50] C. Weidenthaler, A.H. Lu, W. Schmidt, F. Schüth, Micropor. Mesopor. Mat. 2006, 88, 238–243.

[51] Y.P. Guo, D.A. Rockstraw, Micropor. Mesopor. Mat. 2007, 100, 12–19.

[52] K.Y. Foo, B.H. Hameed, J. Anal. Appl. Pyrol. 2012, 98, 123–128.

[53] M.J. Jung, E. Jeong, S. Cho, S.Y. Yeo, Y.S. Lee, J. Colloid Interf. Sci. 2012, 381, 152–157.

[54] W. Xiong, M.X. Liu, L.H. Gan, Y.K. Lv, Y. Li, L. Yang, Z.J. Xu, Z.X. Hao, H.L. Liu, L.W. Chen, J. Power Sources 2011, 196, 10461–10464.

[55] B.E. Conway, Electrochemical supercapacitors: Scientific fundamentals and technological applications, Springer, US, 1999, p. 377–416.

[56] X. Xiang, E. Liu, Y. Wu, Y. Tian, H. Xie, Z. Wu, Y. Zhu, Fuel Cells 2012, 12, 892–897.

[57] S. Biniak, G. Szymański, J. Siedlewski, A. Swiatkowski, Carbon 1997, 1799–1810.

Table 1 – The elemental analysis of the raw material, carbonization and AC samples.

Sample	CHN (wt %)		
	N (%)	C (%)	H (%)
C0	8.39	45.16	5.76
C500	6.81	74.50	2.69
AC700	2.42	63.27	1.67
AC750	2.35	74.87	1.47
AC800	2.09	85.96	1.73
AC850	1.89	88.84	1.36
AC900	1.68	90.25	0.84

Table 2 – Distribution of N species obtained from the deconvolution of the N1s peaks.

Sample	N-6, Pyridinic nitrogen (%) (398.7 ± 0.3eV)	N-5/N-P, Pyrrolic nitrogen, pyridone (%) (400.3 ± 0.3 eV)	N-Q, Quaternary nitrogen (%) (401.4 ± 0.4 eV)	N-X, Oxidized nitrogen (%) (402 ~ 405 eV)
AC700	36.86	55.67	-	8.47
AC750	45.41	46.50	-	8.09
AC800	46.52	41.69	-	11.79
AC850	48.40	39.56	-	12.03
AC900	49.06	38.24	-	12.70

Table 3 – Physical properties of the ACs.

Sample	S_{BET} (m^2/g)	S_{mi} (m^2/g)	V_{tot} (cm^3/g)	V_{mi} (cm^3/g)	S_{me} (%)	V_{me} (%)
AC700	1308	1255	0.586	0.505	4.10	13.81
AC750	1505	1443	0.679	0.588	4.14	13.43
AC800	1586	1499	0.795	0.688	5.47	13.40
AC850	1598	1508	0.862	0.737	5.66	14.49
AC900	1424	1334	0.784	0.663	6.35	15.47

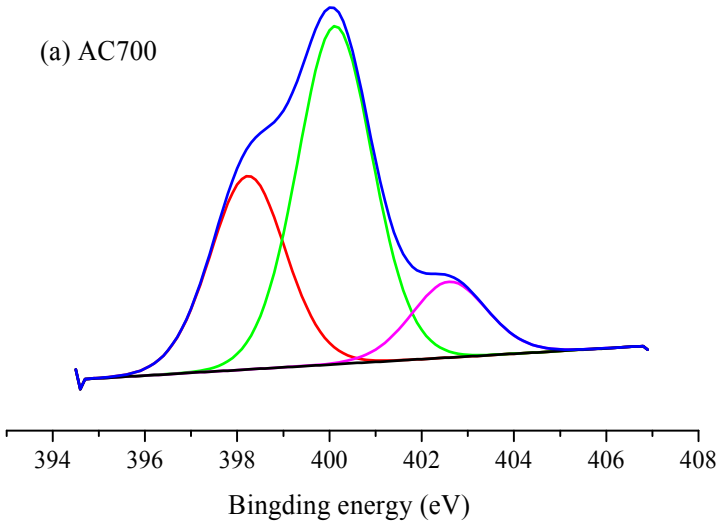

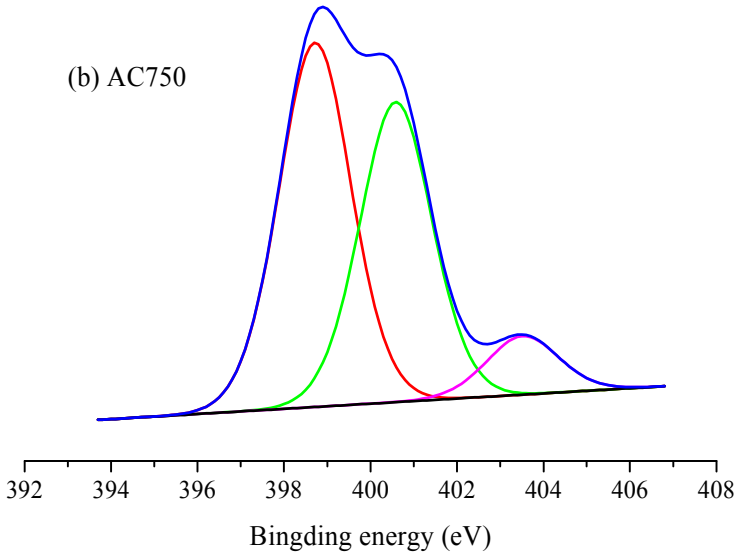

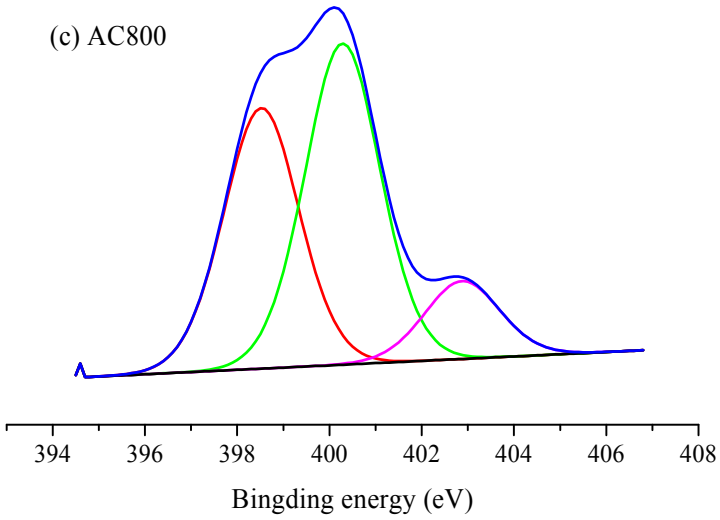

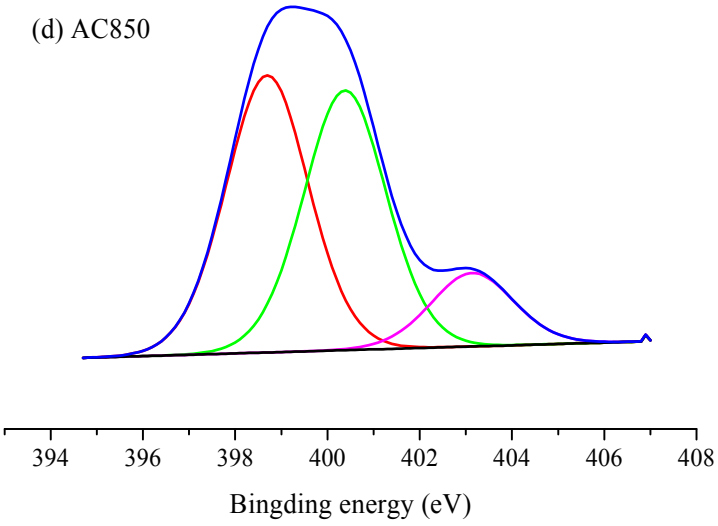

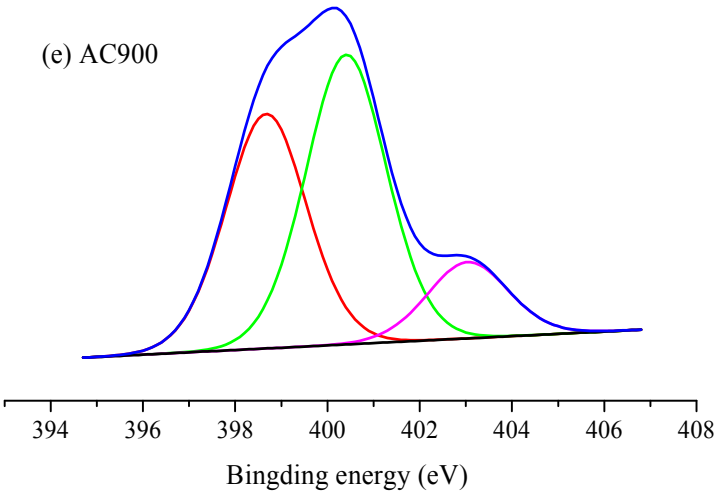

Fig. 1 – Fitted high-resolution XPS N1s spectra of the AC samples.

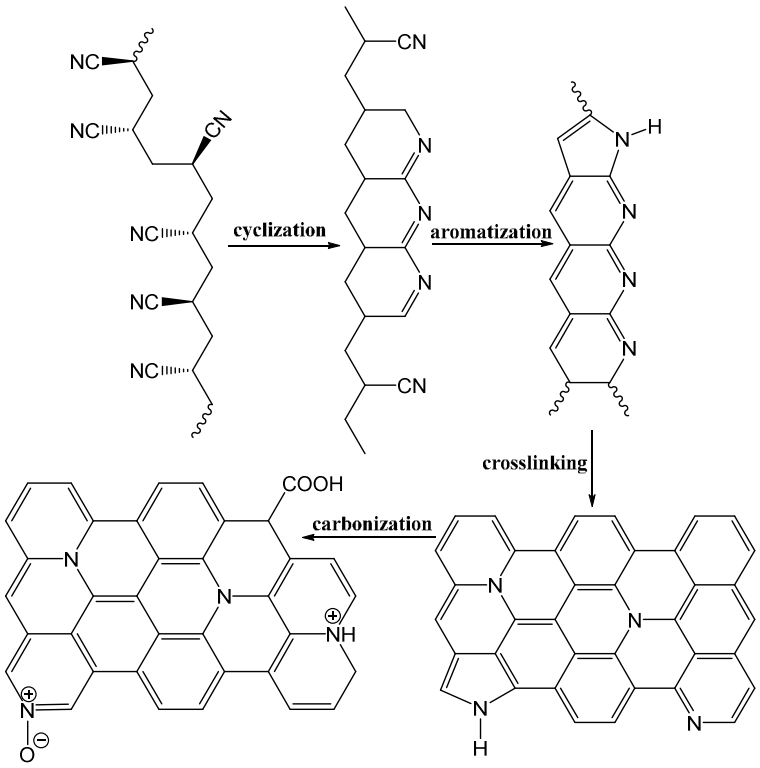

Fig. 2 – Scheme of the graphitization of carbon materials.

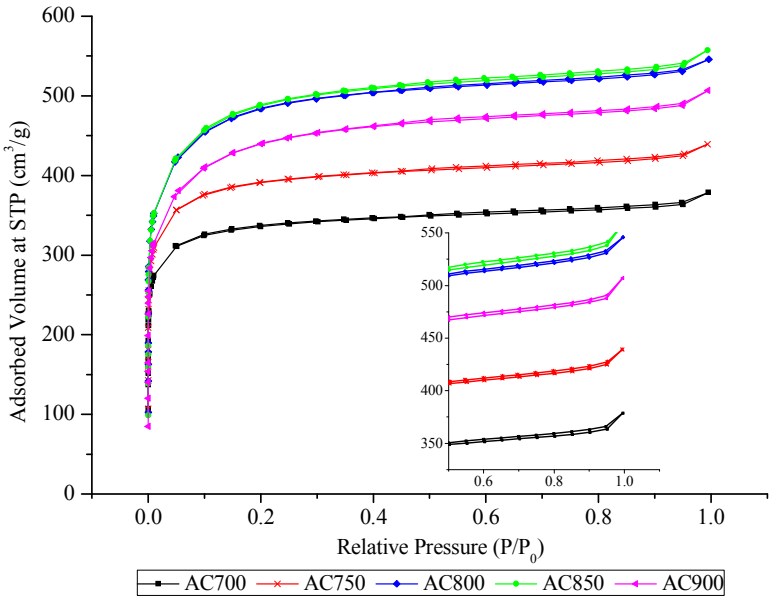

Fig. 3 – Nitrogen adsorption-desorption isotherms for prepared activated carbons by KOH activation.

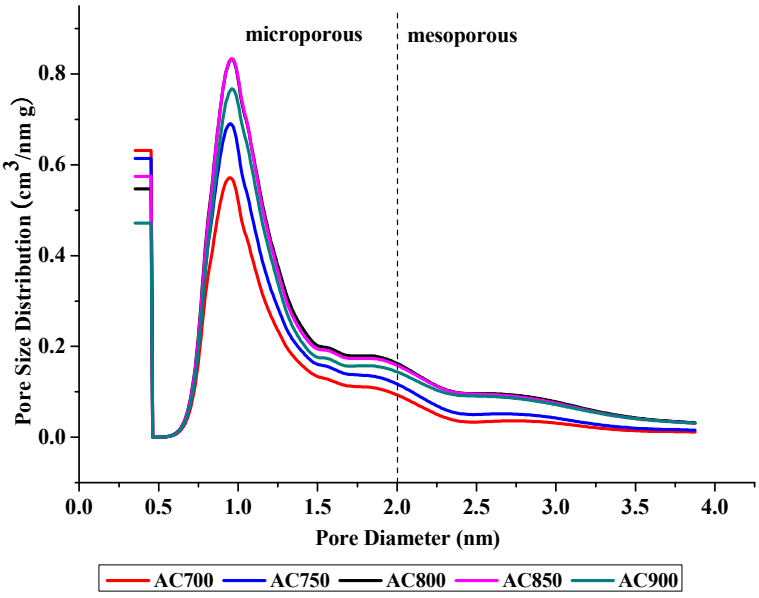

Fig. 4 – Pore size distributions of prepared activated carbons.

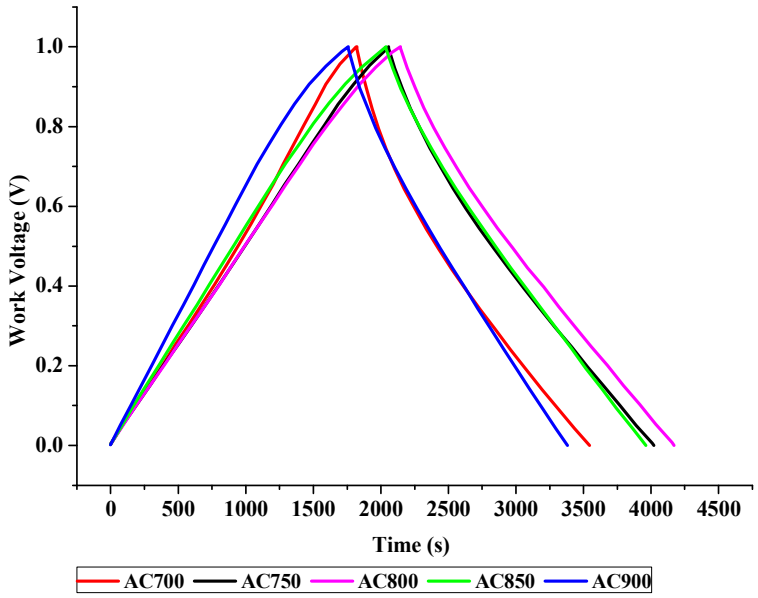

Fig. 5 – Charge-discharge curves of AC electrodes in 7 M KOH at a constant current density of 50 mA/g.

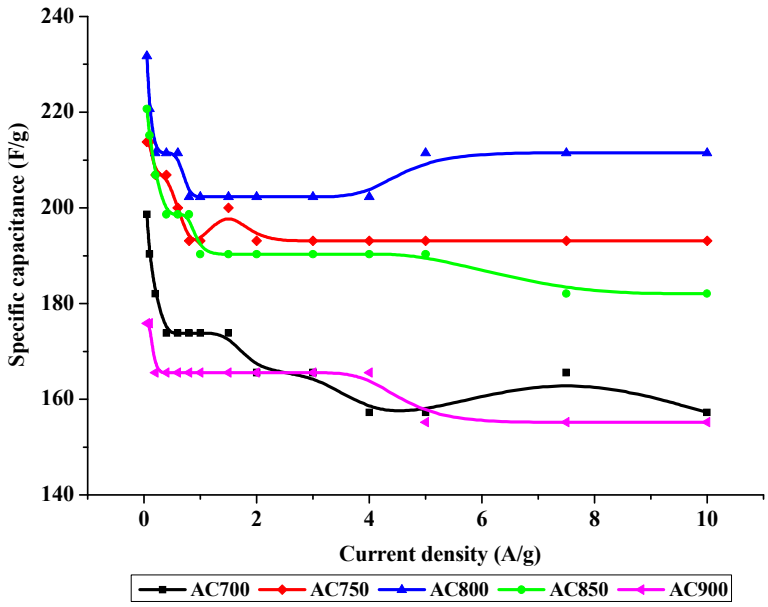

Fig. 6 – Calculated specific capacitance as a function of current density of AC electrodes.

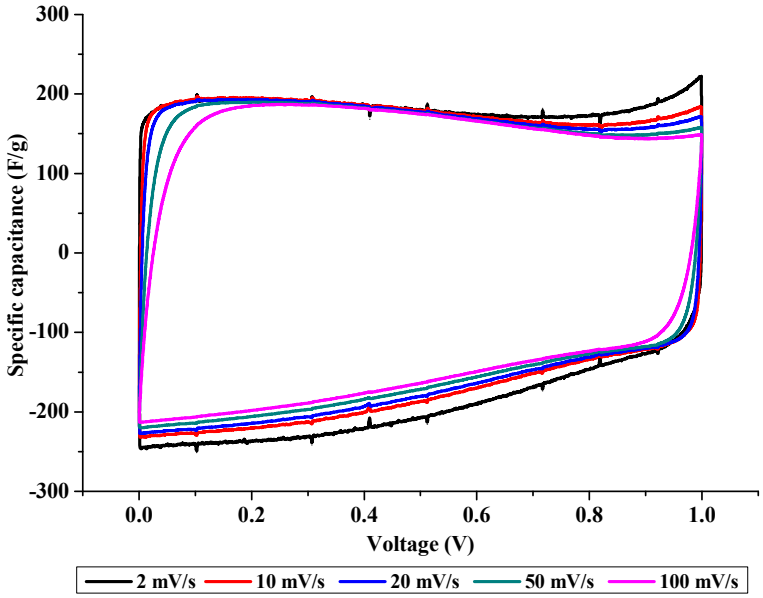

Fig. 7 – Cyclic voltammograms of AC800 electrode in 7 M KOH at different scan rate

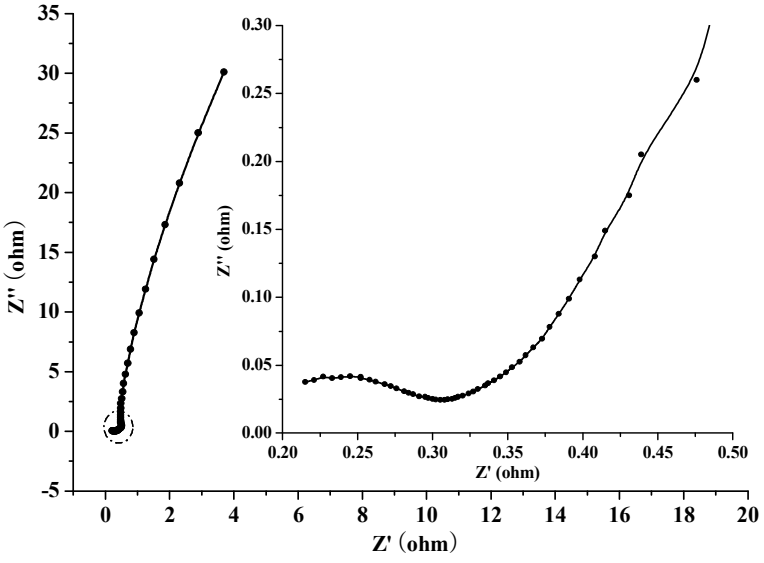

Fig. 8 – Nyquist polt of AC800 electrodes (inset: enlarged high-frequency region of Nyquist polt)